HHMI Author Manuscript
HHMI Author Manuscript
HHMI Author Manuscript

Published as: *Nat Photonics*. 2012 October 1; 6(10): 657–661.

Fluorescence imaging beyond the ballistic regime by ultrasound pulse guided digital phase conjugation

Ke Si[§], **Reto Fiolka**[§], and **Meng Cui**[*]
Howard Hughes Medical Institute, Janelia Farm Research Campus, 19700 Helix Drive, Ashburn, Virginia, 20147, USA

Abstract

Fluorescence imaging has revolutionized biomedical research over the past three decades. Its high molecular specificity and unrivaled single molecule level sensitivity have enabled breakthroughs in a variety of research fields. For *in vivo* applications, its major limitation is the superficial imaging depth as random scattering in biological tissues causes exponential attenuation of the ballistic component of a light wave. Here we present fluorescence imaging beyond the ballistic regime by combining single cycle pulsed ultrasound modulation and digital optical phase conjugation. We demonstrate a near isotropic 3D localized sound-light interaction zone. With the exceptionally high optical gain provided by the digital optical phase conjugation system, we can deliver sufficient optical power to a focus inside highly scattering media for not only fluorescence imaging but also a variety of linear and nonlinear spectroscopy measurements. This technology paves the way for many important applications in both fundamental biology research and clinical studies.

The capability of *in vivo* fluorescence imaging has expanded rapidly over the past few years[1–4]. Despite the progress in spatial resolution[1] and imaging speed[2, 4], the achievable imaging depth in live samples remains very limited[5–7], which has hindered the progress of many research fields[3, 8, 9]. The bottle neck is that only the ballistic component of a light wave has been utilized for imaging, which experiences exponential attenuation due to random scattering in tissues[5, 6]. Here we present fluorescence imaging beyond the ballistic regime by combining single cycle pulsed ultrasound modulation and digital optical phase conjugation. We demonstrate a near isotropic 3D localized sound-light interaction zone. With the exceptionally high optical gain provided by the digital optical phase conjugation system, we can deliver sufficient optical power to a focus inside highly scattering media for not only fluorescence imaging but also a variety of linear and nonlinear spectroscopy measurements.

Users may view, print, copy, download and text and data- mine the content in such documents, for the purposes of academic research, subject always to the full Conditions of use: http://www.nature.com/authors/editorial_policies/license.html#terms

[*]Correspondence and request for materials should be addressed to Meng Cui, 571-209-4136 cuim@janelia.hhmi.org.
[§]Equal contribution

Competing financial interests The authors declare no competing financial interests.

Author Contributions The experiment was designed and implemented by M.C. The fluorescence pattern was created by K.S. The scattering coefficient and the speckle correlation were measured by R.F. All authors contribute to the data analysis and the preparation of the manuscript.
During the editorial process, a similar imaging approach was published[28].

HHMI Author Manuscript HHMI Author Manuscript HHMI Author Manuscript

Controlling wave propagation has been an interesting and important subject in many research fields[7, 10–18]. In principle, if one can reverse both the propagation direction and wavefront of the optical wave originating from a point (i.e. a guide star) inside turbid media, one can form an optical focus at the original point regardless the thickness of the turbid media, a process known as optical phase conjugation (OPC)[11, 12, 19–21]. For imaging, the challenging task is to freely place a guide star at arbitrary locations inside turbid media. Recently, it has been proposed and experimentally demonstrated to use a sound wave to modulate light to create a guide star for OPC[22]. As the scattering of sound waves in tissues is negligible in comparison with light[23], the guide star can be placed at depth far beyond the ballistic regime of light. However, for practical fluorescence imaging, there are two remaining challenges. First, sound and light are both propagating waves in tissues. Even with focused ultrasound, their interaction volume is not 3D confined. Second, given a 3D confined interaction volume, the amount of light that is sound modulated within a highly scattering medium is very small. Thus for practical imaging applications in deep tissues, we need tremendous optical gain ($> 10^3$) for the phase conjugation beam, which cannot be readily provided by a conventional phase conjugation system using photorefractive crystals[10, 24, 25].

Here, we report fluorescence imaging beyond the ballistic regime with < 40 microns spatial resolution. Different from the previous report[22], we use single cycle focused ultrasound pulses and tightly synchronized near-infrared laser pulses to achieve a near isotropic 3D confined interaction volume. The pulsed light and pulsed sound wave are precisely synchronized such that the light wave illuminates the sample only when the single cycle ultrasound pulse propagates to its spatial focus. In such a way, the sound modulation zone is confined in the transverse direction to < 40 microns by the sound focusing element and in the axial direction to < 40 microns by the temporal profile of the single cycle sound pulse convolved with the temporal profile of the laser pulse. To provide sufficient and durable optical power for fluorescence excitation, we employed digital optical phase conjugation[19] (DOPC) to perform phase conjugation.

Figure 1 **a** illustrates schematically the operation of the fluorescence imaging system. A high frequency focused ultrasound transducer launches a single cycle pulse into the sample. A short laser pulse illuminates the sample only when the sound pulse travels through its focus. The wavefront of the frequency shifted light is recorded by the DOPC system using heterodyne interferometry. To measure the fluorescence signal, the DOPC system sends out the phase conjugation beam that precisely propagates to the sound focus. A fluorescence detector measures the power of the emitted fluorescence light. To form a fluorescence image, the entire process is repeated as the acoustic focus is raster scanned inside the sample. The experimental setup (Fig.1 **b**) is described in Methods.

Although without wavefront control the input laser light becomes randomized by scattering, it can still excite fluorescence, resulting in background signals. To measure the background level, we translated the DOPC phase pattern by ~30 pixels both in y and z directions on the SLM (making the DOPC ineffective, see Supplementary Fig. 1 **a–c**). Experimentally we measured the fluorescence signals with and without translating the phase pattern on the SLM and the difference between the two signals was used to represent the fluorescence signal at

HHMI Author Manuscript HHMI Author Manuscript HHMI Author Manuscript

the sound modulation position. We define contrast as the ratio of this signal difference to the background signal, which is shown in the measured images.

To measure the point spread function (PSF) of the system, we dispersed 6 microns diameter fluorescence beads in a 2 mm thick agar slice and sandwiched the fluorescence agar slice between two 2 mm thick scattering tissue phantoms (μ_s=6.42/mm, g=0.9306). The details of the phantom are described in the Supplementary discussion. Figure 2 **a** and **b** show the measured PSF with a sampling step size of 15 microns. The data was resampled with bicubic interpolation, as shown in Fig. 2 **c** and **d**. Gaussian fittings of the cross sections of the PSF (Fig. 2 **e–g**) show that the FWHM of the PSF is 38.6±2.8 microns, 37.9±2.3 microns and 263±90 microns (± 95% confidence bound) along y, z and x directions, respectively. The achieved focus to background ratio (FBR) was ~ 3.7 (Supplementary Fig. 1 **d–e**). A similar experiment was also performed with fixed rat brain slices as the scattering media, as shown in Supplementary Fig. 2.

To verify that the observed fluorescence signals were indeed originating from the ultrasound modulation, we performed a control test by comparing the measurements with and without powering on the amplifier for the ultrasound transducer. We sandwiched a 1 mm thick fluorescence bead agar layer between two 2 mm thick tissue phantoms (g=0.9013, μ_s=10.5/mm). As shown in Supplementary Fig. 3, the signal was gone with the ultrasound transducer disabled.

To demonstrate the fluorescence imaging capability, we used a glass micropipette to manually create an array of 60 microns diameter holes with 120 microns spacing in a 2 mm thick agar slice and injected 6 microns diameter fluorescence beads inside the holes to create a fluorescence pattern. A direct wide field fluorescence image is shown in Fig. 3 **a**. The fluorescence hole array was then surrounded with 2 mm thick tissue phantoms (μ_s=6.42/mm, g=0.9306). Figure 3 **b** shows the fluorescence image of the hole array with tissue phantoms around it. Due to random scattering, the image diffused to ~ 2 mm in diameter and the structure information was completely lost. We raster scanned (step size 30 microns) the position of the acoustic focus and performed DOPC based fluorescence excitation and the raw data is shown in Fig. 3 **c**. The raw data was resampled with bicubic interpolation, as shown in Fig. 3 **d**. For comparison, we show the convolution of the measured PSF (Fig. 2 **c**) with the direct optical image (Fig. 3 **a**) in Fig. 3 **e**. 2D Gaussian fitting for each fluorescence hole is shown in Supplementary Fig. 4. We also imaged samples, in which the fluorescence features were completely embedded in the middle of a 4 mm thick scattering medium (g=0.9013, μ_s=7.09/mm). (Supplementary Fig. 5).

In our experiments, we achieved < 40 microns lateral resolution with near isotropic 3D confined modulation zone. The dependence of the modulation zone on experimental parameters is analyzed in the Supplementary discussion. For applications requiring higher spatial resolution, higher frequency ultrasound transducer can be employed to shrink the modulation zone. In the fluorescence imaging experiments, we used one-photon fluorescence excitation, for which the fluorescence excitation is not 3D confined. The background and the out-of-focus excitations reduce the achievable signal to noise ratio (SNR). However, the background could be dramatically reduced by two-photon excitation at

HHMI Author Manuscript HHMI Author Manuscript HHMI Author Manuscript

the Ti:sapphire wavelength that was employed in this work. In addition, two-photon excitation can further reduce the size of the PSF by ~ $\sqrt{2}$ due to the square dependence of the fluorescence excitation to light intensity.

In this work, the observed FBR is 1.5–4, a value that needs to be improved for practical imaging applications. Previous studies[14, 26] suggest that the achievable FBR is proportional to N_{pixel}/N_{mode}, where N_{pixel} is the number of independently controlled phase pixels on the SLM and N_{mode} is the number of uncorrelated optical modes at the sound modulation zone. An estimation of the theoretical FBR of our system is presented in Supplementary discussion. By iteratively focusing light into the sound modulation zone via DOPC, we can potentially achieve a much smaller sound light interaction volume, leading to better spatial resolution and higher FBR due to the reduced N_{mode} (see Supplementary Discussion). Employing an SLM with less pixel-to-pixel coupling, higher filling factor and diffraction efficiency, and lower temporal phase fluctuation can potentially improve the FBR by more than one order of magnitude. Moreover, the sound modulation zone can be shrunken by using higher frequency sound transducers, reducing N_{mode} and further improving FBR.

In our experiments, we typically acquire 48–96 interferograms and the recording time for one DOPC operation is 1.2–2.4 seconds. We analyzed the SNR's dependence on the camera's parameters in the Supplementary discussion. Using cameras with higher full well charge capacity and frame rate, we can potentially increase the measurement speed by at least one order of magnitude.

For many *in vivo* imaging applications, a transmission configuration is not suitable. However our technique may be extended to measure sound encoded backscattered light[27].

In conclusion, we report fluorescence imaging beyond the ballistic regime with a 3D confined sound modulation zone, high optical gain and < 40 microns lateral resolution in random scattering media. With the capability of focusing sufficient optical power inside random scattering media, our technique can be used for not only fluorescence imaging but also a variety of linear and nonlinear spectroscopy measurements, which is expected to find numerous important biomedical applications.

Methods

Setup

Figure 1**b** shows the setup of the fluorescence imaging system. The laser source is a Q-switched green laser pumped Ti:sapphire laser (Photonics Industries, NY) with 778 nm center wavelength, 10 kHz repetition rate, and 20 ns pulse duration. The laser power is controlled by a half wave plate and a polarizing beam splitter. The laser output was split into two beams. One beam travels through a beam expander and enters the DOPC system. During wavefront recording, it serves as the reference beam for interferometry. During the fluorescence excitation, this beam illuminates the SLM and becomes the phase conjugation beam. The other beam is modulated by an acousto-optic modulator (AOM). The frequency shifted component travels through a beam expander and illuminates the sample during wavefront recording. The sample is housed inside a water chamber with optical windows.

HHMI Author Manuscript HHMI Author Manuscript HHMI Author Manuscript

An ultrasound transducer is mounted on a three-axis translation stage and the sound wave enters the sample from below. The phase conjugation beam is filtered by a bandpass filter before entering the water chamber for fluorescence excitation. The fluorescence emission is filtered by a long-pass filter before entering a camera (Andor iXon 3 888 CCD). In all DOPC experiments the camera was used to measure the fluorescence power by summing all of its pixels with the following two exceptions: in Supplementary Fig. 1 **d** and **e**, a widefield image of a single bead was taken through the clear portion of the sample while it was illuminated with the DOPC system. For the PSF measurement, the fluorescence was recorded from the location of a single bead on the camera while scanning the bead with the ultrasound focus and performing DOPC at each position. The timing and synchronization layout is shown in Supplementary Fig. 6 and the details are discussed below.

Timing and Synchronization

Supplementary Fig. 6 shows the diagram of the timing and synchronization. A delay generator (DG1, Stanford Research DG645) was used as the master clock of the system. It output a 10 MHz TTL pulse train to synchronize an arbitrary waveform generator (AWG, Tektronix AFG3252) and the other delay generator (DG2, Stanford research DG535). DG1 sent out three 10 kHz pulse trains to trigger the Q-switched laser, the arbitrary wavefront generator, and DG2 that controlled the exposure of the CMOS camera. AWG output a 20 ns duration single cycle sinusoidal signal that changed sign with every pulse (Supplementary Fig. 7 **c**) to drive the ultrasound transducer. The ultrasound frequency was centered at 50,005,000 Hz (50MHz + 5kHz) and the pulse repetition rate was 10 kHz. The extra 5 kHz makes sure that the residual interferences (aliasing) sampled by any two consecutive laser pulses are exactly out of phase by 180 degrees and hence are canceled out by capturing an even number (i.e. 100) of laser pulses. AWG also output a CW 50,004,990 Hz sinusoidal signal for driving the AOM. The beating between the ultrasound transducer and the AOM was 10 Hz and the CMOS camera ran at 40 Hz, controlled by DG2. For every 25 ms, the CMOS spent the first 10 ms for exposure and during the remaining 15 ms transferred the data to a computer. The driving signals for the ultrasound transducer and the AOM were amplified to 140–160 Vp-p and 30 Vp-p, respectively.

Supplementary Material

Refer to Web version on PubMed Central for supplementary material.

Acknowledgements

The authors thank Charles Shank, Ying Min Wang and Changhuei Yang for helpful discussions, Tsai-Wen Chen for instructions on the micropipette puller and Amy Hu for preparing the fixed rat brain slices. The research is supported by Howard Hughes Medical Institute.

References

1. Betzig E, et al. Imaging intracellular fluorescent proteins at nanometer resolution. Science. 2006; 313:1642–1645. [PubMed: 16902090]
2. Planchon TA, et al. Rapid three-dimensional isotropic imaging of living cells using Bessel beam plane illumination. Nature Methods. 2011; 8:417–U468. [PubMed: 21378978]

HHMI Author Manuscript HHMI Author Manuscript HHMI Author Manuscript

3. Wilt BA, et al. Advances in Light Microscopy for Neuroscience. Annual Review of Neuroscience. 2009; 32:435–506.
4. Huisken J, Swoger J, Del Bene F, Wittbrodt J, Stelzer EHK. Optical sectioning deep inside live embryos by selective plane illumination microscopy. Science. 2004; 305:1007–1009. [PubMed: 15310904]
5. Theer P, Denk W. On the fundamental imaging-depth limit in two-photon microscopy. Journal of the Optical Society of America a-Optics Image Science and Vision. 2006; 23:3139–3149.
6. Theer P, Hasan MT, Denk W. Two-photon imaging to a depth of 1000 mu m in living brains by use of a Ti : Al2O3 regenerative amplifier. Optics Letters. 2003; 28:1022–1024. [PubMed: 12836766]
7. Tang J, Germain RN, Cui M. Superpenetration optical microscopy by iterative multiphoton adaptive compensation technique. Proceedings of the National Academy of Sciences. 2012; 109:8434–8439.
8. Supatto W, McMahon A, Fraser SE, Stathopoulos A. Quantitative imaging of collective cell migration during Drosophila gastrulation: multiphoton microscopy and computational analysis. Nat. Protocols. 2009; 4:1397–1412. [PubMed: 19745822]
9. Mempel TR, Henrickson SE, von Andrian UH. T-cell priming by dendritic cells in lymph nodes occurs in three distinct phases. Nature. 2004; 427:154–159. [PubMed: 14712275]
10. Feinberg J, Hellwarth RW. Phase-conjugating mirror with continous-wave gain. Optics Letters. 1980; 5:519–521. [PubMed: 19701292]
11. Yariv A, Yeh P. Phase conjugate optics and real-time holography. Ieee Journal of Quantum Electronics. 1978; 14:650–660.
12. Leith EN, Upatniek J. Holographic imagery through diffusing media. Journal of the Optical Society of America. 1966; 56:523–&.
13. Vellekoop IM, Mosk AP. Universal optimal transmission of light through disordered materials. Physical Review Letters. 2008; 101
14. Vellekoop IM, Mosk AP. Focusing coherent light through opaque strongly scattering media. Optics Letters. 2007; 32:2309–2311. [PubMed: 17700768]
15. Lerosey G, De Rosny J, Tourin A, Fink M. Focusing beyond the diffraction limit with far-field time reversal. Science. 2007; 315:1120–1122. [PubMed: 17322059]
16. Katz O, Small E, Bromberg Y, Silberberg Y. Focusing and compression of ultrashort pulses through scattering media. Nature Photonics. 2011; 5:372–377.
17. Vellekoop IM, van Putten EG, Lagendijk A, Mosk AP. Demixing light paths inside disordered metamaterials. Optics Express. 2008; 16:67–80. [PubMed: 18521133]
18. Hsieh CL, Pu Y, Grange R, Laporte G, Psaltis D. Imaging through turbid layers by scanning the phase conjugated second harmonic radiation from a nanoparticle. Optics Express. 2010; 18:20723–20731. [PubMed: 20940968]
19. Cui M, Yang C. Implementation of a digital optical phase conjugation system and its application to study the robustness of turbidity suppression by phase conjugation. Optics Express. 2010; 18:3444–3455. [PubMed: 20389354]
20. Cui M, McDowell EJ, Yang CH. Observation of polarization-gate based reconstruction quality improvement during the process of turbidity suppression by optical phase conjugation. Applied Physics Letters. 2009; 95
21. Cui M, McDowell EJ, Yang C. An in vivo study of turbidity suppression by optical phase conjugation (TSOPC) on rabbit ear. Opt. Express. 2010; 18:25–30. [PubMed: 20173817]
22. Xu XA, Liu HL, Wang LV. Time-reversed ultrasonically encoded optical focusing into scattering media. Nature Photonics. 2011; 5:154–157. [PubMed: 21532925]
23. Wang LV. Multiscale photoacoustic microscopy and computed tomography. Nature Photonics. 2009; 3:503–509. [PubMed: 20161535]
24. Yaqoob Z, Psaltis D, Feld MS, Yang C. Optical phase conjugation for turbidity suppression in biological samples. Nature Photonics. 2008; 2:110–115. [PubMed: 19492016]
25. Feinberg J, Heiman D, Tanguay AR, Hellwarth RW. Photorefractive effects and light-induced charge migration in barium-titanate. Journal of Applied Physics. 1980; 51:1297–1305.
26. Vellekoop, IM. Ph.D. thesis, Univ. Twente. 2008. Controlling the Propagation of Light in Disordered Scattering Media.

27. Lai PX, Xu X, Liu HL, Suzuki Y, Wang LHV. Reflection-mode time-reversed ultrasonically encoded optical focusing into turbid media. Journal of Biomedical Optics. 2011; 16

28. Wang YM, Judkewitz B, DiMarzio CA, Yang C. Deep-tissue focal fluorescence imaging with digitally time-reversed ultrasound-encoded light. Nature Communications. 2012; 3:928.

HHMI Author Manuscript HHMI Author Manuscript HHMI Author Manuscript

HHMI Author Manuscript
HHMI Author Manuscript
HHMI Author Manuscript

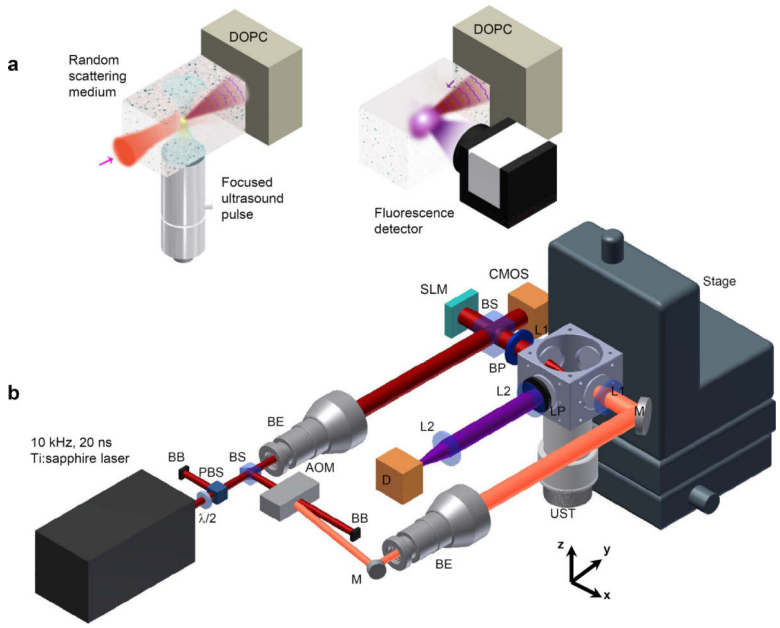

Figure 1.

a Experimental scheme of fluorescence microscopy by single cycle ultrasound pulse guided DOPC. **b** Experiment setup. λ/2, half wave plate; PBS, polarizing beam splitter; BB, beam block; BS, non-polarizing beam splitter; BE, beam expander; M, mirror; BP, band-pass filter; LP, long-pass filter; L1, f = 35 mm lens; L2, f = 50 mm lens; D, fluorescence detector; Stage, 3-axis motorized translation stage. The pixel size of both the SLM and the CMOS camera is 8 microns. The distance from the sound focus to the SLM is 305 mm.

HHMI Author Manuscript

HHMI Author Manuscript

HHMI Author Manuscript

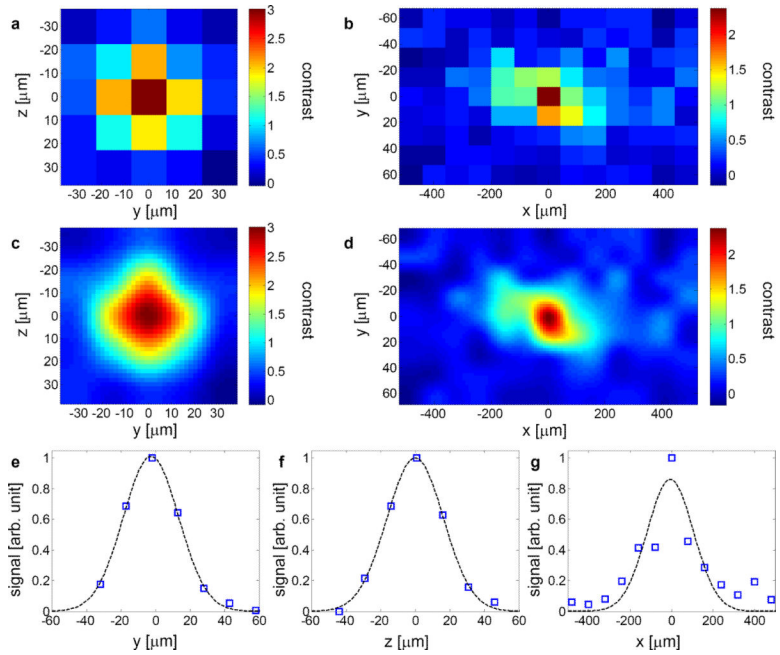

Figure 2.

a Measured transverse PSF through 2 mm thick tissue phantoms (μ_s=6.42/mm, g=0.9306). **b** Measured axial PSF. **c** and **d** are the corresponding images resampled with bicubic interpolation. **e**–**g** Gaussian fitting of the measured PSF.

HHMI Author Manuscript

HHMI Author Manuscript

HHMI Author Manuscript

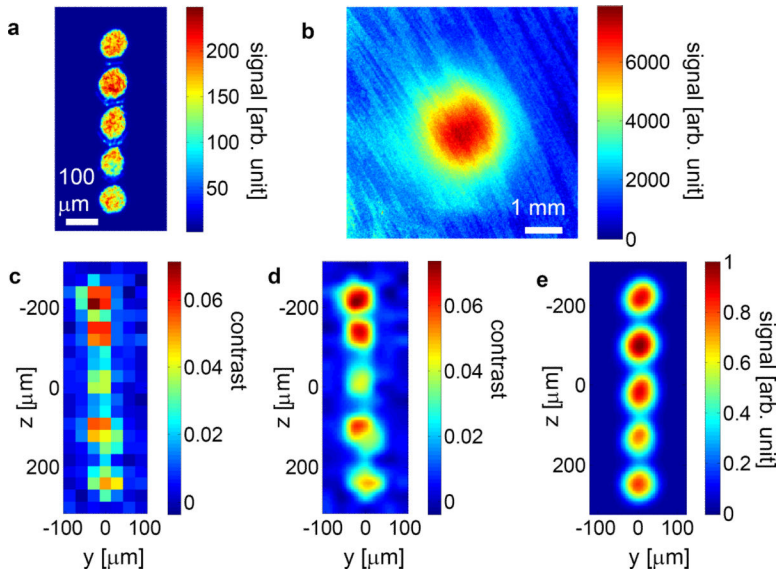

Figure 3.

a Direct optical imaging of the fluorescence hole array without tissue phantoms. **b** Direct optical imaging of the fluorescence hole array surrounded by 2 mm thick tissue phantoms (μ_s=6.42/mm, g=0.9306). **c** Image acquired with ultrasound pulse guided DOPC through tissue phantoms. The laser power on the sample was 25 mW during sound modulation and 10 mW during fluorescence excitation. **d** Bicubic interpolation of **c**. **e** 2D convolution of **a** with Fig. 2 **c**. The tissue phantoms were aligned parallel to the yz plane in Fig. 1 **b**.